Mechanical strength and microstructure of oxygen ion-implanted Al films

S. Bader
Department of Materials Science and Engineering, Stanford University, Stanford, California 94305

P. A. Flinn
Intel Corporation, SC9-45, 2250 Mission College Boulevard, Santa Clara, California 95124, and Department of Materials Science and Engineering, Stanford University, Stanford, California 94305

E. Arzt
Max-Planck-Institut für Metallforschung, Institut für Werkstoffwissenschaft, Stuttgart, Germany

W. D. Nix
Department of Materials Science and Engineering, Stanford University, Stanford, California 94305

(Received 1 March 1993; accepted 6 October 1993)

The influence of finely dispersed, stable particles on the mechanical strength and microstructure of Al films on Si substrates has been studied. Aluminum oxide particles were produced in Al films by oxygen ion implantation, and the grain size was increased by a laser reflow treatment. Transmission electron microscopy (TEM) was employed to observe the oxide particles and the grain structure in the films after subsequent annealing, and the wafer curvature technique was used to study the deformation properties of the films as a function of temperature. Significant particle strengthening was obtained in the coarse-grained films in tension as well as in compression. In the as-deposited and ion-implanted films a very fine grain size of only 0.35 μm is stabilized after annealing which causes considerable softening of the film in compression at higher temperature because of the enhancement of grain boundary and volume diffusion controlled relaxation mechanisms. However, in tension at low temperature these films show high stresses comparable to those of the laser reflowed and ion-implanted films. The results are discussed in the light of TEM observations.

I. INTRODUCTION

Aluminum is widely used as an interconnect material in microelectronic devices. Failure of the interconnect lines in these devices can severely limit reliability. In some cases these failures can be caused by insufficient mechanical strength of the materials involved. Thermal stresses arise in interconnect lines during device fabrication and in service at elevated temperatures because of large differences in thermal expansion between aluminum and the silicon substrate. These stresses can relax by dislocation glide and diffusional deformation processes,[1] which, in turn, can cause hillock or void formation to occur and may result in short or open circuits.

Electromigration is another important failure mechanism for conductor lines. The discovery that electromigration causes stresses to develop in conductor lines has led to the suggestion that mechanical strength may be an important factor in determining electromigration failure resistance.[2,3] Recent theories suggest that materials which can sustain higher hydrostatic stresses will show better resistance to electromigration failure. Thus, the development of interconnect materials (especially aluminum alloys) with higher mechanical strength may be a promising way to improve reliability.

A well-established method for strengthening bulk materials involves the formation of ordered precipitates or dispersoid particles, which act as obstacles to dislocation motion.[4] In such materials plastic flow can occur only if the dislocations are able to cut through, bow between, or climb over the particles. These processes all require higher stresses and/or longer times and thus lead to strengthening effects.

Because of their higher electromigration resistance, Al(Si)–Cu and Al(Si)–Ti alloys are used as interconnections in microelectronic devices. These alloys contain precipitate phases that could be used for strengthening. However, in both systems the precipitates tend to coarsen and to segregate at grain boundaries and triple points.[5] Also, the precipitates in the Al(Si)–Cu system dissolve with increasing temperature and impart full strengthening only at lower temperatures ($T < 200$ °C).[6] To overcome these limitations we have attempted to strengthen aluminum by creating a fine dispersion of Al_2O_3 particles; the aim of this effort was to achieve a strengthening effect at all temperatures.

 © 1994 Materials Research Society

Aluminum oxide particles were created in sputter deposited aluminum films by oxygen ion implantation. Because the heat of formation of Al_2O_3 is very high (1676 kJ/mol),[7] the activation barrier for nucleation of Al_2O_3 dispersoids is easily overcome and fine Al_2O_3 dispersoids are formed. In order to separate the strengthening effects of dispersoids from those of grain boundaries, some of the aluminum films were subjected to a "laser reflow treatment". Here the aluminum film is momentarily melted by a laser beam, and after subsequent solidification[8] a large grain size is produced. By combining oxygen ion implantation with laser reflow treatments, it was possible to study the effects of both Al_2O_3 dispersoids and grain size on the strength properties of aluminum films.

In this paper we report on the microstructure created in aluminum films by oxygen ion implantation and/or the laser reflow treatment. We also report on the strength of these films, as determined by substrate curvature measurements during thermal cycling, and we discuss the results in terms of the observed microstructures.

II. EXPERIMENTAL PROCEDURES

Pure aluminum films, 0.5 μm in thickness, were magnetron sputtered onto unheated, thermally oxidized, (100) oriented silicon wafers, 100 mm in diameter. The sputter system base pressure was 4.0×10^{-7} Torr. The deposition rate was 1.8 nm/s at an Ar pressure of 3.0×10^{-3} Torr. The grain size of the as-deposited aluminum film was found to be 0.6 μm using transmission electron microscopy (TEM). We refer to these films as "standard" aluminum films.

Some of the films were subjected to a laser reflow treatment using an XMR 7100 system with an XeCl laser operating at 308 nm. The base pressure for this system was 3.6×10^{-6} Torr. The wafers were heated to 400 °C, and a laser beam with a spot size of 3.6×3.6 mm^2 was rastered over the wafer. An energy dose of 3.2 J/cm^2 was used and the laser pulse duration was of the order of tens of nanoseconds. The resulting grain size was found to be 5.6 μm using light microscopy (LM) and the intercept method. We use for these films the designation LR.

The oxygen ion implantation was done, using a Varian DF-4 ion implanter, in five partial implants, ranging in energy from 10 keV to 190 keV and in dose from 5.0×10^{15} ions/cm^2 to 4.5×10^{16} ions/cm^2; this implantation profile was used to achieve a relatively uniform oxygen concentration through the thickness of the film. The final oxygen concentration was approximately 3.0 at.%, corresponding to a maximum of 3 vol.% Al_2O_3. The oxygen ion implantation treatment had no effect on the grain size before annealing. We refer to films that received the oxygen ion implantation treatment as OII. For those films that were laser reflowed prior to oxygen ion implantation we use the designation LR + OII.

The strength properties of these films were studied by measuring the biaxial stress in the film as a function of temperature using the substrate curvature method.[9] This technique is based on the fact that stressed thin films bend the substrate elastically. The curvature of the wafer was measured using a laser-based optical lever device. The relation between the curvature, $1/R_\sigma$, induced by the biaxial stress in the film, σ is given by

$$\sigma = \frac{E_s t_s^2}{6(1 - \nu_s)t_f} \frac{1}{R_\sigma} \tag{1}$$

where E_s, ν_s, and t_s are, respectively, Young's modulus, Poisson's ratio, and the thickness of the substrate, and t_f is the thickness of the film. To determine $1/R_\sigma$, the curvature of the bare wafer must be subtracted from the measured curvature of the film-substrate composite. Using this method, the stress in the film was measured as a function of temperature through several heating and cooling cycles with a constant heating and cooling rate of 6 °C per minute.

Transmission electron microscopy was done to study the microstructure of the films. Plan-view TEM samples were prepared by drilling a disk, 3 mm in diameter, out of the wafer and grinding it down to 100 μm. After dimpling to a thickness of 10 μm in the center of the sample, ion milling was used to remove the rest of the Si and to thin the Al film to an appropriate thickness. Cross-section TEM specimen preparation was done as described in Ref. 10.

III. RESULTS

A. Strength properties

Figures 1 and 2 show stress-temperature curves for all of the different process conditions. In Fig. 1 the stress temperature response is shown for the second thermal cycle for both the standard film and oxygen ion implanted film (OII). Figure 2 shows the same kind of results for a laser reflowed film (LR) and for a laser reflowed film that had also been subjected to oxygen ion implantation (LR + OII). All of these curves have a similar shape, indicative of the elastic and plastic processes that occur during thermal cycling.

As the sample is heated above room temperature, the film deforms first elastically and the stress decreases linearly. The slope of the elastic line is given by

$$\frac{d\sigma}{dT} = \frac{E_f}{1 - \nu_f} \Delta\alpha, \tag{2}$$

where E_f and ν_f are, respectively, Young's modulus and Poisson's ratio of the film, and $\Delta\alpha$ is the difference between the thermal expansion coefficients of the substrate and the film. Eventually the stress in the

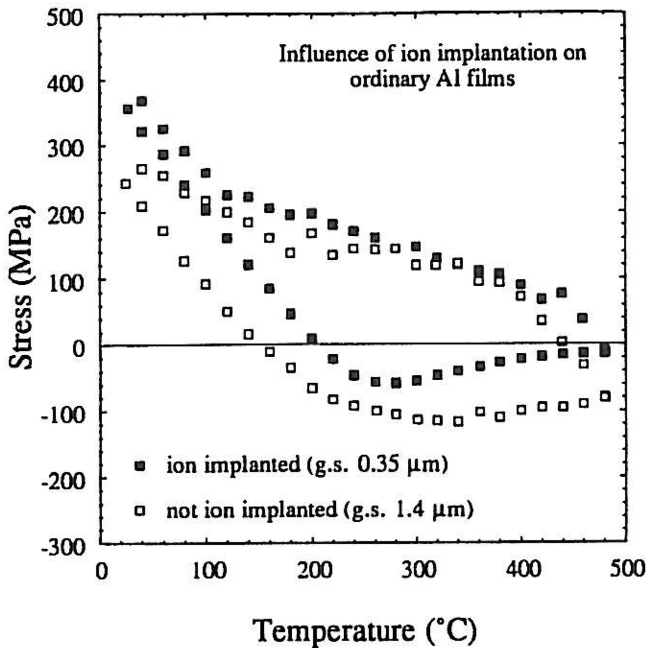

FIG. 1. Variation of stress with temperature for the second cycle of a standard Al film (No. 1.1) and an ion-implanted film without the laser reflow treatment (OII) (No. 2.1).

film becomes compressive, and the stress-temperature curve starts to deviate from the elastic line, indicative of plastic yielding. The same elastic-plastic sequence occurs on cooling. To confirm the results, two films of each kind were tested. In Table I, four prominent stresses are tabulated for the first three cycles of each film. Here σ_{max} is the maximum compressive stress in the cycle and σ_{end} is the compressive stress at the highest temperature (before cooling back to room temperature). Also, $\sigma_{plateau}$ is the average tensile stress in the temperature interval where the stress is nearly constant, usually between 180 and 220 °C. This plateau appeared in most of the stress-temperature curves. Finally, $\sigma_{40\,°C}$ is the tensile stress at 40 °C, at the end of the cycle (maximum tensile stress).

The laser reflowed films are about 20 MPa stronger in compression and about 50 MPa stronger in tension than the standard aluminum films. The laser reflowed films that were also ion implanted (LR + OII) show, in both compression and tension, the highest strengths of all four kinds of films. By comparison, the ion-implanted films (OII) show very low yield stresses in compression, and the flow stress decreases rapidly between the temperature corresponding to σ_{max} (T_{max}) and that corresponding to σ_{end} (T_{end}). In one film the stress was observed to decrease to near zero. However, in tension these films show strengths that are equivalent to those of the ion-implanted films that had been laser reflowed (LR + OII). Further, the strengthening effect observed in these films (OII) on cooling from the plateau regime to room temperature is quite pronounced. In this part of the curve the rate at which the tensile stress increases with decreasing temperature indicates that plastic flow is not occurring and that the film is deforming only elastically.

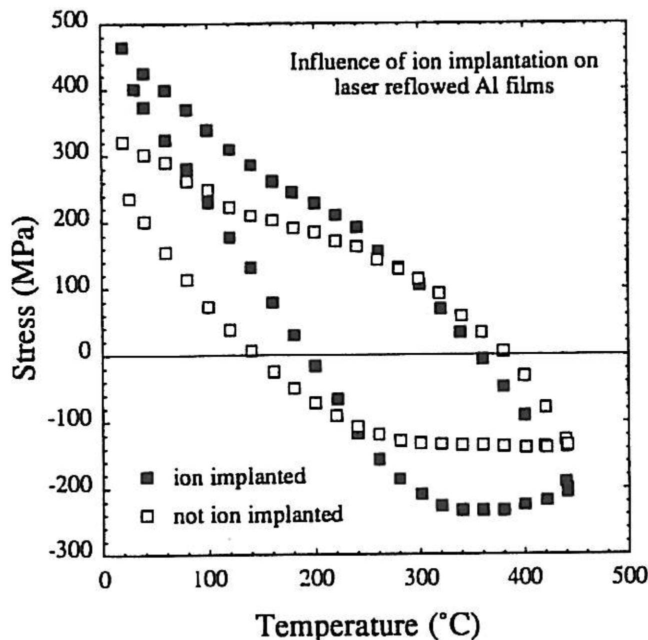

FIG. 2. Variation of stress with temperature of the second cycle of a laser reflowed film (No. 3.1) and a laser reflowed film that had also been ion implanted (LR + OII) (No. 4.1).

B. Grain structures

In order to be able to understand the mechanical properties of these films, it is necessary to examine their microstructures. Light microscopy, scanning electron microscopy (SEM), and transmission electron microscopy were used to evaluate the grain size and microstructure of the films. The grain sizes, both before and after the first thermal cycle, are shown in Table II for each of the different process treatments. In subsequent thermal cycles the grain size remained almost constant. The grain size of the laser reflowed films was stable and did not change during the first thermal cycle. By contrast, the standard aluminum films exhibit grain growth from the as-deposited grain size of 0.6 μm to a stable grain size of 1.4 μm. This increase in grain size is accompanied by a decrease in the compressive flow strength of the film, as expected. Both kinds of films that were ion implanted (OII and LR + OII) show a decrease in grain size during the first thermal cycle, indicating recrystallization, most likely driven by the high density of defects created by ion implantation. As will be discussed later, the microstructures of these films indicate that recrystallization was not complete.

TABLE I. Characteristic stresses for the first three thermal cycles for each of the four different process conditions.

Process conditions	Sample no.	Thermal cycle no.	Compression (MPa)		Tension (MPa)	
			σ_{max}	σ_{end}	$\sigma_{plateau}$	$\sigma_{40\ °C}$
Standard aluminum films	1.1	1	148	100	147	271
		2	80	80	135	265
		3	105	105	138	267
	1.2	1	99	83*	145	258
		2	126	85	145	245
		3	135	97	140	233
Oxygen ion-implanted films	2.1	1	140	45	220	410
		2	98	43	240	425
		3	98	45	220	385
	2.2	1	118	20	186	343
		2	58	13	195	368
		3	65	17	184	358
Laser reflowed films	3.1	1	...	...	...	...
		2	138	137*	...	301
		3	142	142*	...	307
	3.2	1	137	104	190	362
		2	123	104	197	337
		3	120	97	175	302
Laser reflowed films with oxygen ion implantation	4.1	1	277	230*	...	440
		2	233	205*	...	425
		3	246	225*	...	407
	4.2	1	206	177	220	357
		2	183	152	192	349
		3	172	149	200	354

σ_{max} corresponds to the maximum compressive stress observed in the thermal cycle. σ_{end} is the compressive stress at the highest temperature reached during the thermal cycle which was 480 °C, except for the cycles indicated by *, which were taken to 440 °C. $\sigma_{plateau}$ is the "plateau" stress observed in tension, usually between 180 °C and 220 °C. $\sigma_{40\ °C}$ is the tensile stress at 40 °C, at the end of the cooling part of the cycle.

C. Dispersoids

Figure 3 shows a bright-field (BF) TEM micrograph of the microstructure after the first thermal cycle of a laser reflowed film that had been subjected to oxygen ion implantation (LR + OII). Many so-called "coffee bean" contrasts and moiré patterns are visible in the micrograph. These "coffee bean" contrasts are caused by the strain field of small particles and not by dislocation loops (which may be formed by irradiation damage due to ion milling[11]), because they did not appear in TEM samples of laser reflowed films prepared in the same way. In addition, it was noted that particles also form at grain boundaries and grow preferentially there. Figure 4 shows a dark-field (DF) micrograph of the same film (LR + OII) after four thermal cycles. The density of particles is higher than after the first cycle (Fig. 3). Some of the particles have grown and changed their contrast from the "coffee bean" type to small moiré patterns, visible as 2–3 parallel black and white stripes. Particles could also be found in the ion-implanted films that had not been laser reflowed (OII). Figures 5 and 6 show BF TEM micrographs of those films after the fourth cycle. The grain boundaries are densely decorated with particles and surrounded by particle-denuded zones (Fig. 5). The particles at grain boundaries are mostly

TABLE II. Grain sizes for different process treatments.

Process conditions	Grain size	Technique used
Standard aluminum film		
As-deposited	0.6 μm	TEM
After first annealing cycle	1.4 μm	TEM
Oxygen ion-implanted film		
As-deposited	0.6 μm	TEM
After first annealing cycle	0.35 μm	TEM
Laser reflowed film		
As-deposited	5.6 μm	LM, SEM
After first annealing cycle	5.6 μm	LM, SEM
Laser reflowed film with oxygen ion implantation		
As-deposited	5.6 μm	LM, SEM
After first annealing cycle	3.5 μm	LM, SEM

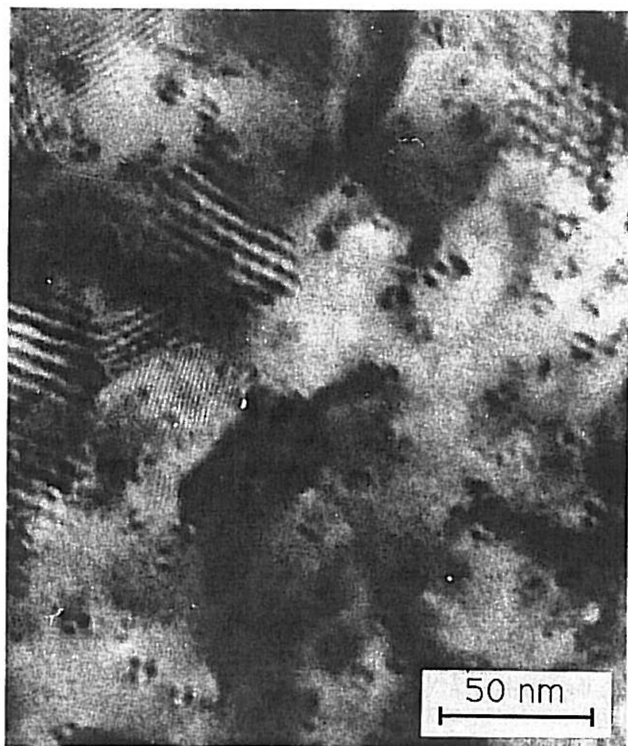

FIG. 3. BF plan-view TEM photograph of a laser reflowed and ion-implanted film (LR + OII) (No. 4.1) after the first cycle.

visible as black dots. Under suitable reflection conditions 2–3 black and white stripes are visible inside the dots,

FIG. 4. DF plan-view TEM photograph of a laser reflowed and ion-implanted film (LR + OII) (No. 4.1) after the fourth cycle.

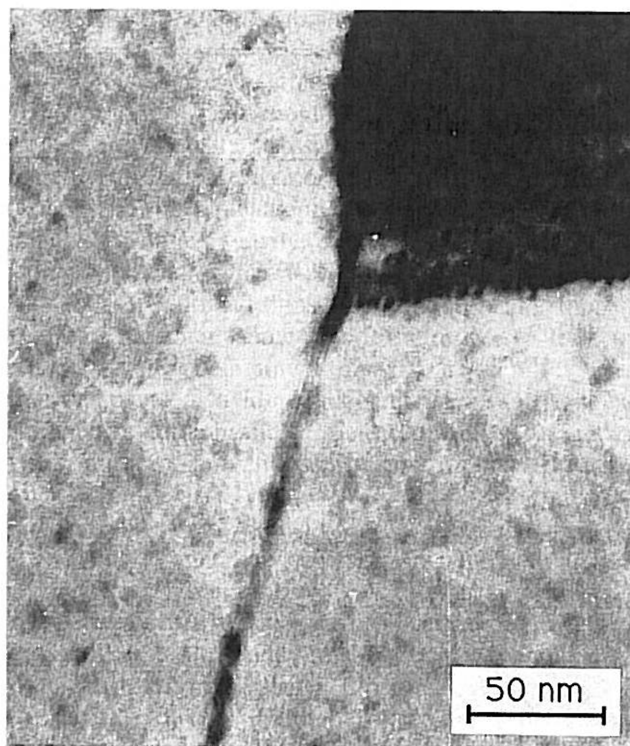

FIG. 5. BF plan-view TEM photograph of an ion-implanted film without the laser reflow treatment (OII) (No. 2.1) after the fourth cycle.

appearing much like the particles inside the grains of ion-implanted films that had been laser reflowed (LR + OII).

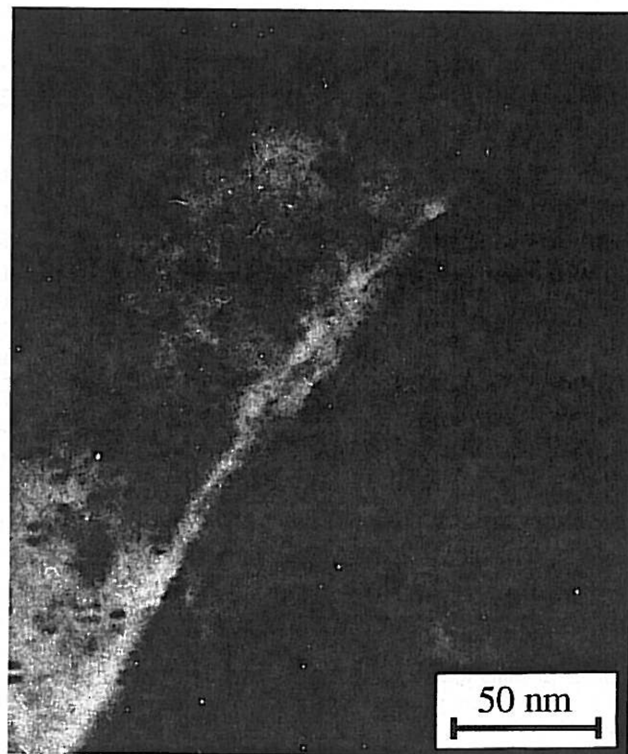

FIG. 6. BF plan-view TEM photograph of an ion-implanted film without the laser reflow treatment (OII) (No. 2.1) after the fourth cycle.

Inside the grains one sees primarily small particles visible as "coffee bean" contrasts. The stable grain size of only 0.35 μm in these films suggests that the grain boundaries are pinned by the oxide particles, especially if the particles are small and numerous. This pinning effect results in small recrystallized grains in the films with ion implantation (OII).

The moiré patterns in the plan-view TEM samples of the ion-implanted films (OII) suggest that the grain structure of these films is no longer columnar. Figure 7 shows a cross-section micrograph of an ion-implanted film (a), together with the corresponding convergent beam diffraction pattern (DP) of the indicated columnar grain (b). Columnar grains are still present, but inside smaller grains are visible. The diffraction pattern shows that the normally sharp reflections are spread out or are replaced by some weaker, but distinct, reflections, which all lie within a narrow angular range on the Debye–Scherrer rings. This indicates clearly that subgrains and subgrain boundaries have formed within the columnar grains. The fact that the grain size decreased in both kinds of the ion-implanted films (OII and LR + OII) by a factor of one half suggests that recrystallization occurred. However, the presence of these subgrains indicates that recrystallization was not complete. The lattice may have recovered from the lattice damage produced by the ion implantation treatment by forming subgrain boundaries, because the columnar grain boundaries were pinned early by the oxide particles.

There is additional evidence for particles in the diffraction pattern. In almost all of the ion-implanted films (OII and LR + OII), some weak extra Debye–Scherrer rings could be found. A ring corresponding to a lattice d-spacing of about 1.4 Å was seen in all of the films with the ion implantation treatment. The d-spacing of 1.4 Å corresponds to a variety of Al_2O_3 modifications such as $\alpha-Al_2O_3$ (corundum)[12] or $\eta-Al_2O_3$,[13] for which this is the strongest reflection. In the ion-implanted films that had been laser reflowed (LR + OII), additional rings with d-spacings of 1.97 Å and 1.136 Å, which correspond to $\eta-Al_2O_3$, were present. However, the ion-implanted films (OII) showed an additional reflection near 1.6 Å, which corresponds very well to $\alpha-Al_2O_3$.

After an anneal for one week between temperatures of 180 and 380 °C, all rings corresponding to $\eta-Al_2O_3$ appear in the ion-implanted films as well as in the films that had received no ion implantation. This suggests that the surface oxide layer, which is amorphous at short annealing times, starts to crystallize during longer anneals at elevated temperatures.

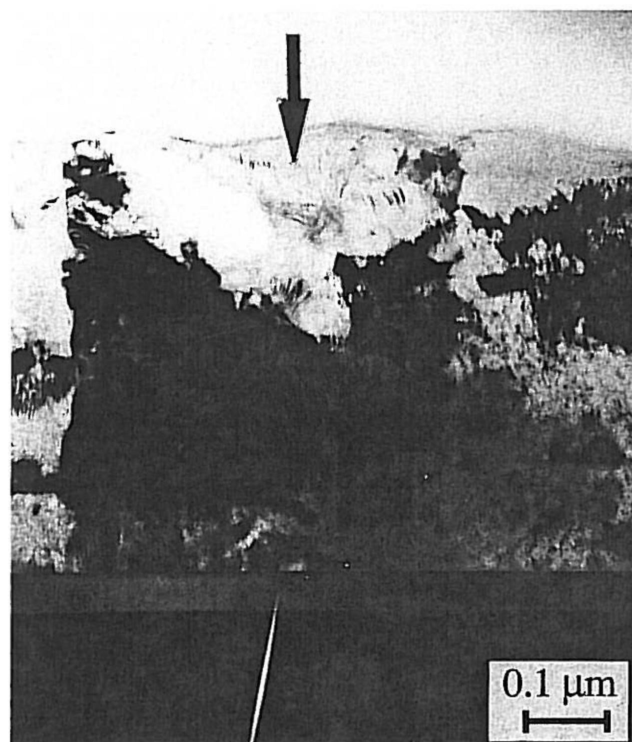

(a)

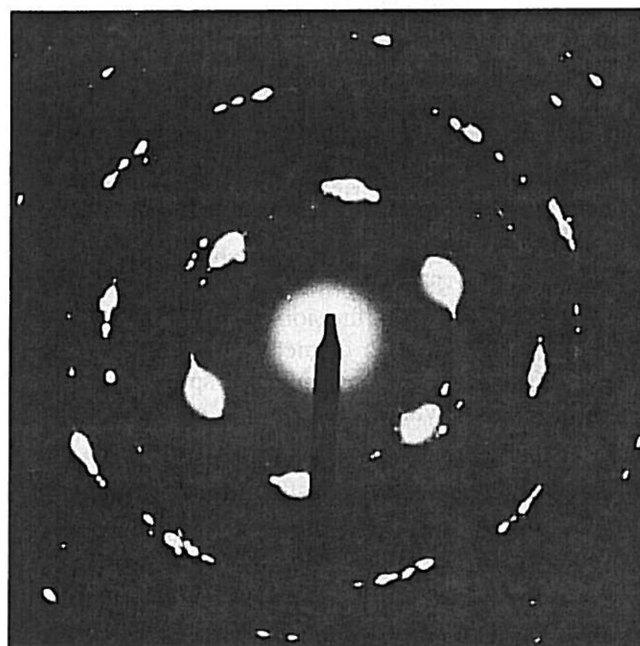

(b)

FIG. 7. (a) BF cross section TEM photograph of an ion-implanted film without the laser reflow treatment (OII) (No. 2.1) after the first cycle; (b) DP of the columnar grain indicated in (a).

D. Hillocks

SEM and surface profile measurements with a Dektak IIA stylus profilometer were used to investigate the surface morphology and especially the hillocking behavior of the films. The hillocking behavior of both kinds of films with the ion implantation treatment is

significantly different from that of the films without the ion implantation treatment. After the first cycle the ion-implanted films (OII and LR + OII) already show more and much larger hillocks than their counterparts without the ion implantation treatment. In films without ion implantation the number of hillocks increases with an increasing number of cycles. In the films with ion implantation treatment (OII and LR + OII), the number of hillocks seems to remain constant after the first cycle, though they grow in size with each successive thermal cycle. After four cycles the hillocks have a height between 1 and 2 μm and a lateral dimension of about 3 μm (Figs. 8 and 9). The height of the hillocks in the films without ion implantation is at most 1 μm and the lateral dimension is about the same. The laser reflowed films show the least hillocking of all four kinds of films, an observation already reported by Venkatraman *et al.*[14] After the first cycle there are almost no hillocks visible, and after the fourth cycle only a few can be seen. While the hillocks in ion-implanted films (OII and LR + OII) grow exclusively by diffusion out of grain boundaries, about 50% of the hillocks in the films without ion implantation seem to be whole grains which grow or deform out of the film. As a result, the surface of the ion-implanted films, in between the hillocks, seems to be smoother overall than the surface of the films without the ion implantation treatment. Grain boundary grooving develops in the laser reflowed films during laser reflow processing and increases with further annealing. This grooving is especially pronounced in laser reflowed films that were also ion implanted (LR + OII); in these films cavities form at triple points and small cracks develop along some grain boundaries. These damage processes are probably driven by the relatively high stresses in these films.

On the surface of the ion-implanted films (OII), loop-like grooves with a diameter of about 0.8 μm are formed. These loops may indicate specially oriented grain boundaries which tend to show grooving.

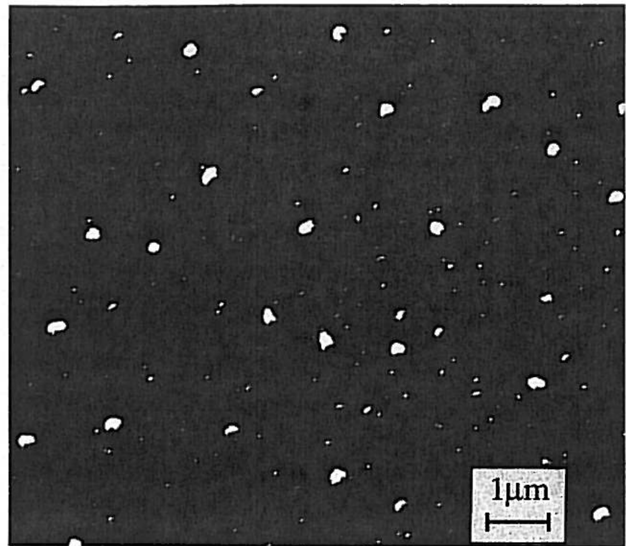

FIG. 8. SEM photograph of an ion-implanted film without the laser reflow treatment (OII) (No. 2.1) after the fourth cycle.

IV. DISCUSSION

For most films, the first thermal cycle showed a higher maximum compressive stress, σ_{max}, and a higher compressive stress, σ_{end}, than the following cycles. For the standard aluminum films this is probably caused by the grain growth that occurs during the first thermal cycle. TEM observations showed that the grain size changes from 0.6 μm in the as-deposited condition to 1.4 μm after the first thermal cycle. The corresponding change in the stress-temperature behavior follows the Hall–Petch relation, whereby the flow stress decreases with increasing grain size. For both kinds of ion-implanted films (OII and LR + OII), the decrease in compressive strength that occurs between the first and second thermal cycles is most likely due to the annealing-out of ion-induced point defects during the first thermal cycle as well as due to the change in grain size. For the only laser reflowed films, no significant changes in strength occur between the first and second cycles, because the laser reflow process produces a stable microstructure. Subsequent thermal cycles for each particular film produce very similar stress-temperature curves. However, different films with the same special treatments often show quite different stress temperature curves, suggesting that the laser reflow and the ion implantation treatments are not very reproducible.

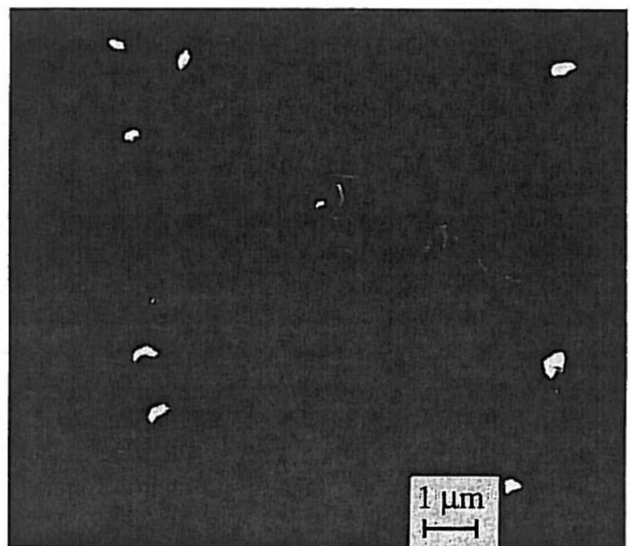

FIG. 9. SEM photograph of a laser reflowed and ion-implanted film (LR + OII) (No. 4.2) after the first cycle.

Our finding that the laser reflowed films are stronger than the standard aluminum films both in compression and tension is in disagreement with previous results of Venkatraman *et al.*[14] This discrepancy can be rationalized by considering the different process and experimental conditions. The laser reflow parameters for Venkatraman's films were slightly different and resulted in a much larger grain size of 22 μm for 0.48 μm thick films; this compares with a grain size of only about 5.6 μm for our films. Following the Hall–Petch relation, our films should be stronger due to grain boundary inhibition of dislocation motion. Furthermore, we performed our wafer curvature experiments in an N_2 atmosphere rather than in air. This may have led to a thinner oxide layer on the films, which allows grain boundary-diffusion controlled relaxation mechanisms to take place more easily. These mechanisms would decrease the stresses more in the films without the laser reflow treatment because of the smaller grain size in these films.

The films with the oxygen ion implantation treatment (OII and LR + OII) show very high stresses in tension (Figs. 1 and 2). The slopes of the curves during cooling at low temperatures are almost equal to the elastic slope. This means that at low temperatures the yield strength is not reached. Especially in the ion-implanted films that were not laser reflowed (OII), the transition from the "plateau" to the steep slope is very pronounced. The laser reflowed films with ion implantation (LR + OII) show very high stresses in compression as well. In these films, dispersion strengthening occurs in tension as well as in compression. Grain boundary diffusion related softening processes are not dominant because of the large grain size. Figure 10 shows a weak beam (111, 333) TEM micrograph of one of these films. Dislocations pinned at particles are visible.

The ion-implanted films that were not laser reflowed (OII) are very weak in compression, especially at higher temperatures between $T_{\max}$ and T_{end}, where they show a considerable amount of softening, and, in tension, above 300 °C they show stresses below those of the standard aluminum films. The presence of stable particles in these films does not ensure high compressive strengths at elevated temperatures. The small grain size of only 0.35 μm allows the stresses to be relaxed by diffusion controlled processes, in spite of the presence of the particles. The high density of large hillocks supports this view. By contrast, dispersion strengthening is evident in tension below 150 °C, most likely caused both directly by particle-dislocation interactions and indirectly by stabilizing a small grain size (Hall–Petch strengthening).

In an effort to understand the effects of diffusional relaxation on the deformation properties of these films, stress-temperature curves were calculated for the case in which only grain boundary (Coble) and volume (Nabarro–Herring) diffusion controlled creep were allowed to occur. The differential equation to be solved is

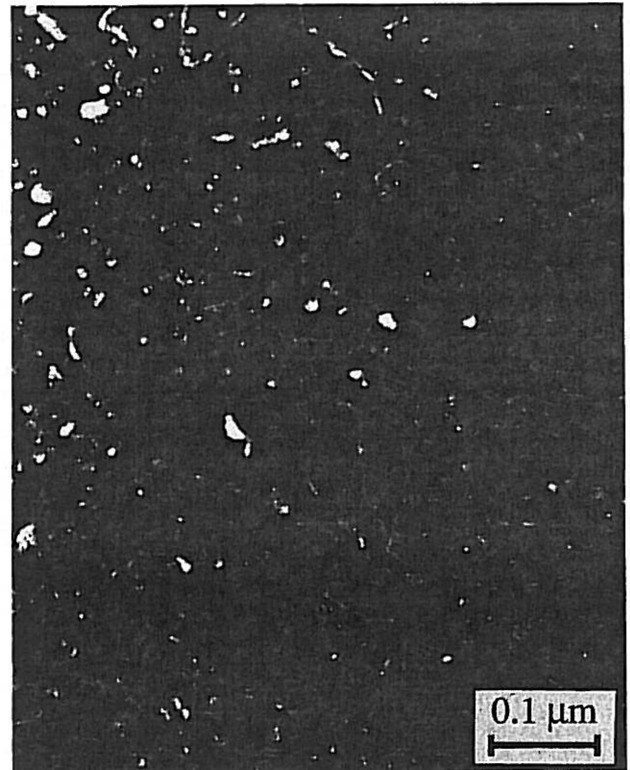

FIG. 10. Weak beam plan-view TEM photograph of a laser reflowed and ion-implanted film (LR + OII) (No. 4.1) after the first cycle.

$$\frac{d\sigma}{dT} = \frac{E_f}{1-\nu_f}\left(\Delta\alpha - \dot{\epsilon}(\sigma, T, d, h)\frac{1}{\dot{T}}\right), \qquad (3)$$

where $\dot{T}$ is the heating/cooling rate and $\dot{\epsilon}$ is the diffusion controlled biaxial strain rate (negative in compression) defined by

$$\dot{\epsilon} = \dot{\epsilon}_{gb} + \dot{\epsilon}_v, \qquad (4)$$

where $\dot{\epsilon}_{gb}$ and $\dot{\epsilon}_v$ are the grain boundary and volume controlled diffusional creep rates, respectively. We used the equations derived first by Gibbs[15] for the case of diffusional creep in thin films:

$$\dot{\epsilon}_{gb} = 12\frac{\delta D_{gb}\Omega}{dh^2 \mathrm{k}T}\sigma \qquad \delta D_{gb} = \delta D_{gb}^0 \exp(-Q_{gb}/\mathrm{k}T) \qquad (5)$$

$$\dot{\epsilon}_v = 7.5\frac{D_v\Omega}{dh\mathrm{k}T}\sigma \qquad D_v = D_v^0 \exp(-Q_v/\mathrm{k}T), \qquad (6)$$

where h is the film thickness, d is the in-plane grain size, and all of the other terms have their usual meanings for diffusional analysis. Because these equations do not account for the adherence of the film to the substrate

(they assume that the grains are free to slide easily with respect to the substrate), they greatly overpredict the amount of stress relaxation that can occur at high temperatures. Nevertheless, the simple analysis of Gibbs can be used to provide some insight into the temperature at which the diffusional relaxation begins to occur. Mathematica 2.0[16] was used to solve Eq. (3) in conjunction with Eqs. (4)–(6). The calculations were made for a lateral grain size of 0.35 μm, a film thickness of 0.5 μm, and a heating/cooling rate of 6 °C/min, using the properties of pure aluminum given by Frost and Ashby.[17]

For the case that the total strain rate is the sum of the grain boundary and volume diffusional strain rates, on cooling from high temperatures, the stress in the film remains near zero down to 120 °C, where it begins to increase rapidly with decreasing temperature. The abrupt rise in stress below 120 °C occurs because the diffusional processes are too slow to relax the stress at these temperatures. We note that the experimental curve (Fig. 1) also rises abruptly at 120 °C, indicating that all relaxation processes are inhibited below that temperature. Thus, the diffusional model correctly predicts the temperature at which relaxation processes are effectively stopped. For heating, the stress decreases rapidly and is zero above 100 °C. The model predictions do not compare well with experiment at high temperatures because, as mentioned before, the equations do not account for the adherence of the grains in the film to the substrate.[18] Further, the texture may reduce the effective diffusion coefficient of the grain boundaries and the number of grain boundaries that can act as sources and sinks for vacancies and in this way inhibit the amount of diffusional relaxation that can occur. For the case that the total strain rate is only the volume diffusional strain rate, on cooling, the stress rises already around 230 °C. This, together with the agreement cited above, clearly indicates that grain boundary diffusion plays an important role in the relaxation. However, a quantitative model describing the shape and the asymmetry of the measured stress/temperature curves is still lacking. Work along this line is currently in progress.

Hillocks are believed to be formed by grain boundary diffusion. The high density of large hillocks observed in these films (OII) supports the conclusion that grain boundary diffusion processes are involved in the relaxation. That grain boundary diffusion contributes significantly to the relaxation also helps to explain the tension-compression strength asymmetry. This can be partly explained by considering that the material which diffuses out of the film and forms the hillocks on heating cannot easily diffuse back into the film on cooling. An oxide layer may form on the hillocks, thereby preventing diffusion along the surface to supply grain boundary diffusion back into the film. This would cause the kind of strength asymmetry observed in the experiment.

A comparison of the hillocking behavior of the ion-implanted films with and without laser reflowing indicates that high stresses do not necessarily lead to extensive hillocking. The ion-implanted films with laser reflowing (LR + OII) show very high compressive stresses upon heating, but only a few hillocks. In contrast, the ion-implanted films without laser reflowing (OII) show very low compressive stresses, but a high hillock density. The low stresses that are observed may be related to a high hillock density. Figure 9 shows that, despite the high stresses present in the laser reflowed films, hillocks grow at only a few of the grain boundaries. This suggests that special sites, such as specially oriented grain boundaries or grains, are necessary to form hillocks.[19] In the ion-implanted films without laser reflowing (OII), the grain size is smaller and the grain boundary density higher, resulting in a high density of specially oriented grain boundaries that can support hillock growth.

V. SUMMARY AND CONCLUSION

Oxygen ion implantation changes the microstructure and the stress/temperature deformation behavior of aluminum films considerably. Precipitation of very fine Al_2O_3 particles was detected after the first thermal cycle. The particles continue to grow in the following cycles, preferentially at the grain boundaries. The corresponding evolution of the grain structure in the ion-implanted films can be described as follows. The high defect density created in the films by ion implantation causes recrystallization to occur on thermal cycling. Grain growth, which follows recrystallization, slows down very quickly due to the drag on grain boundaries caused by particles. In this way a stable grain size of only 0.35 μm developed in the ion-implanted films that had not received the grain coarsening laser reflow treatment (OII). A stable grain size of 3.5 μm was formed in the ion-implanted films that had been laser reflowed (LR + OII). Further recovery of the high defect density probably occurs by the formation of subgrains within the columnar grains.

The high tensile and compressive stresses in the laser reflowed and ion implanted films can be attributed to dispersion strengthening by dislocation-dispersoid interactions. By contrast, the very low stresses in compression and the extensive softening at higher temperatures in the ion-implanted films without laser reflowing (OII) can be attributed to diffusion-controlled stress relaxation mechanisms, which are enhanced because of the small grain size. The high tensile stresses in these films at low temperatures are probably caused by both direct (dislocation-dispersoid interactions) and indirect (stabi-

lized fine grains) particle strengthening. A quantitative model for these effects is still lacking.

For the laser reflowed and ion-implanted films (LR + OII), we expect improved electromigration resistance because of the larger grain size and better mechanical properties. For the ion-implanted films without laser reflowing (OII), initial tests did not show an improved electromigration resistance,[20] probably because of the very small grain size which enhances the electromigration flux along grain boundaries.

ACKNOWLEDGMENTS

The authors would like to thank Ann F. Marshall for her help with the TEM work. Support for S. Bader was provided by the Deutsche Forschungsgemeinschaft (DFG). E. Arzt and W. D. Nix acknowledge the financial support for this collaboration, in the form of the "Max-Planck-Prize", awarded by the Alexander-von-Humbold-Stiftung and the Max-Planck-Gesellschaft.

REFERENCES

1. M. F. Doerner and W. D. Nix, *CRC Critical Reviews in Solid State and Materials Sciences (Stresses and Deformation Processes in Thin Films on Substrates*, Vol. 14), (CRC Press, Boca Raton, FL, 1988), pp. 225–268.
2. J. R. Blech and K. L. Tai, Appl. Phys. Lett. **30**, 387 (1977).
3. E. Arzt and W. D. Nix, J. Mater. Res. **6**, 731 (1991).
4. L. M. Brown and R. K. Ham, *Strengthening Methods in Crystals,* edited by A. Kelly and R. B. Nicholson (Applied Science Publisher, London, 1971), p. 126.
5. J. E. Sanchez, Jr., L. T. McKnelly, and J. W. Morris, Jr., in *Phase Transformation Kinetics in Thin Films,* edited by M. Chen, M. O. Thompson, R. Schwarz, and M. Libera (Mater. Res. Soc. Symp. Proc. **230**, Pittsburgh, PA, 1992).
6. P. H. Townsend, Ph.D. Dissertation, Stanford University (1987).
7. Hollemann-Wiberg, Lehrbuch der Anorganischen Chemie, Walter deGryter (1976), p. 649.
8. S. Chen and E. Ong, Proc. SPIE's 1989 Symp. on Microelectronic Integrated Processing: Conference on Laser/Optical Processing of Electronic Materials, Santa Clara, CA, Oct. 10–11 (1989).
9. P. A. Flinn, in *Thin Films: Stresses and Mechanical Properties,* edited by J. C. Bravman, W. D. Nix, D. M. Barnett, and D. A. Smith (Mater. Res. Soc. Symp. Proc. **130**, Pittsburgh, PA, 1989), p. 41.
10. J. C. Bravman and R. Sinclair, J. Electron Microsc. Technique **1**, 53 (1984).
11. J. W. Edington, *Practical Electron Microscopy in Materials Science* (TechBooks, Herndon, VA, 1976), p. 213.
12. Natl. Bur. Stand. (U.S.), Circ. 539, 93 (1960).
13. Stumpf *et al.*, Ind. Eng. Chem. **42**, 1398 (1950).
14. R. Venkatraman, S. Chen, and J. C. Bravman, J. Vac. Sci. Technol. A **9** (4), 2536 (Jul/Aug 1991).
15. G. B. Gibbs, Philos. Mag. **13**, 589 (1966).
16. Wolfram Research Inc., Champaign, IL.
17. H. J. Frost and M. F. Ashby, Deformation-Mechanism Maps (Pergamon Press, Oxford, 1982), ISBN 0-08-029337-9.
18. M. S. Jackson and Che-Yu Li, Acta Metall. **30**, 1993–2000 (1982).
19. J. E. Sanchez, Jr., and E. Arzt, Scripta Metall. **27**, 285 (1992).
20. E. Arzt, O. Kraft, J. Sanchez, S. Bader, and W. D. Nix, in *Thin Films: Stresses and Mechanical Properties III,* edited by W. D. Nix, J. C. Bravman, E. Arzt, and L. B. Freund (Mater. Res. Soc. Symp. Proc. **239**, Pittsburgh, PA, 1992), p. 677.